ARMY RESEARCH LABORATORY

ARL

Analysis of Adhesively Bonded Ceramics Using an Asymmetric Wedge Test

by Andres Bujanda, Craig Copeland, Jessica Dibelka, Aaron Forster, Larry Holmes, Robert Jensen, Wendy Kosik, Steven McKnight, Stephen Koellhoffer, and John Gillespie, Jr.

ARL-TR-4665   **December 2008**

NOTICES

Disclaimers

The findings in this report are not to be construed as an official Department of the Army position unless so designated by other authorized documents.

Citation of manufacturer's or trade names does not constitute an official endorsement or approval of the use thereof.

Destroy this report when it is no longer needed. Do not return it to the originator.

Army Research Laboratory

Aberdeen Proving Ground, MD 21005-5069

Analysis of Adhesively Bonded Ceramics Using an Asymmetric Wedge Test

Andres Bujanda, Craig Copeland, Jessica Dibelka, Aaron Forster, Larry Holmes, Robert Jensen, Wendy Kosik, and Steven McKnight
Weapons and Materials Research Directorate, ARL

Stephen Koellhoffer and John Gillespie, Jr.
University of Delaware

REPORT DOCUMENTATION PAGE			*Form Approved* *OMB No. 0704-0188*

Public reporting burden for this collection of information is estimated to average 1 hour per response, including the time for reviewing instructions, searching existing data sources, gathering and maintaining the data needed, and completing and reviewing the collection information. Send comments regarding this burden estimate or any other aspect of this collection of information, including suggestions for reducing the burden, to Department of Defense, Washington Headquarters Services, Directorate for Information Operations and Reports (0704-0188), 1215 Jefferson Davis Highway, Suite 1204, Arlington, VA 22202-4302. Respondents should be aware that notwithstanding any other provision of law, no person shall be subject to any penalty for failing to comply with a collection of information if it does not display a currently valid OMB control number.
PLEASE DO NOT RETURN YOUR FORM TO THE ABOVE ADDRESS.

1. REPORT DATE *(DD-MM-YYYY)* December 2008	2. REPORT TYPE Final	3. DATES COVERED (From - To) January 2006–August 2006

4. TITLE AND SUBTITLE Analysis of Adhesively Bonded Ceramics Using an Asymmetric Wedge Test	5a. CONTRACT NUMBER
	5b. GRANT NUMBER
	5c. PROGRAM ELEMENT NUMBER
6. AUTHOR(S) Andres Bujanda, Craig Copeland, Jessica Dibelka, Aaron Forster, Larry Holmes, Robert Jensen, Wendy Kosik, Steven McKnight, Stephen Koellhoffer,[*] and John Gillespie, Jr.[*]	5d. PROJECT NUMBER AH84
	5e. TASK NUMBER
	5f. WORK UNIT NUMBER

7. PERFORMING ORGANIZATION NAME(S) AND ADDRESS(ES) U.S. Army Research Laboratory ATTN: AMSRD-ARL-WM-MA Aberdeen Proving Ground, MD 21005-5069	8. PERFORMING ORGANIZATION REPORT NUMBER ARL-TR-4665
9. SPONSORING/MONITORING AGENCY NAME(S) AND ADDRESS(ES)	10. SPONSOR/MONITOR'S ACRONYM(S)
	11. SPONSOR/MONITOR'S REPORT NUMBER(S)

12. DISTRIBUTION/AVAILABILITY STATEMENT
Approved for public release; distribution is unlimited.

13. SUPPLEMENTARY NOTES
[*]University of Delaware, Center for Composite Materials, Newark, DE 19716

14. ABSTRACT

Quantitative determination of adhesive performance when bonding to ceramic substrates has traditionally been a challenge. The brittleness of ceramic materials limits the ability to easily machine these substrates into the specific geometries required for rigorous adhesive fracture energy measurements. In this research, a mixed-mode loading scheme was implemented using an asymmetric wedge test configuration to study the effects of adhesion, promoting surface treatments on fracture energy and bond line durability of titanium bonded to alumina using a structural epoxy film adhesive. This testing scheme limited bending to the more compliant titanium and minimized deformations in the thicker alumina. Additionally, machining the alumina was avoided due to the relative simplicity of the testing configuration. X-ray photoelectron spectroscopy showed that sandblasting the ceramic surface yielded improved reactivity toward the sol-gel adhesion promoter used in this study, which resulted in increased hot/wet bond durability. Weibull modulus calculations and field emission-scanning electron microscopy imaging of the ceramic fracture surfaces showed that surface flaws induced while sandblasting the ceramic did not decrease the flexural strength.

15. SUBJECT TERMS
ceramics, surface treatment, adhesive, asymmetric wedge, sol-gel, XPS

16. SECURITY CLASSIFICATION OF:			17. LIMITATION OF ABSTRACT	18. NUMBER OF PAGES	19a. NAME OF RESPONSIBLE PERSON Andres Bujanda
a. REPORT UNCLASSIFIED	b. ABSTRACT UNCLASSIFIED	c. THIS PAGE UNCLASSIFIED	UL	32	19b. TELEPHONE NUMBER *(Include area code)* 410-306-0680

Standard Form 298 (Rev. 8/98)
Prescribed by ANSI Std. Z39.18

Contents

List of Figures

List of Tables

Acknowledgments

1. Introduction

Ceramics as a material class offer superior compressive strengths, thermal stability, low coefficient of thermal expansion (CTE), hardness, and abrasion resistance that lend themselves to a wide range of applications. In particular, ceramic materials perform well as strike faces in lightweight armor assemblies, but their weak tensile fracture strength eliminates use as a stand-alone replacement for traditional metals. To incorporate the advantages of ceramics over metals and meet rising demands for lighter armor, a laminated multimaterial composite structure is required. This structure may utilize a ductile backing plate to counteract the weak tensile fracture strengths and delay the onset of catastrophic failure during a ballistic event (*1*, *2*). In addition, weight requirements often dictate that armor assemblies carry structural load, which often requires using a high-quality polymeric adhesive bond between the ceramic and backing plate (*3*). Polymeric adhesive bonding of backing plate candidate materials, such as metals and fiber-reinforced composites, has been widely studied, and the bond strength and durability properties are well characterized (*4*, *5*). However, specialized methodologies for quantifying adhesive bond strengths in ceramic materials are limited due to unique experimental challenges, as ceramic materials are extremely difficult to machine into test geometries specified by ASTM, JIS, and ISO standards.

The first critical aspect of adhesive bonding to ceramics is the difficulty of machining and handling ceramic materials. Machining ceramics into tensile testing specimen geometries is costly and difficult, especially along the gage length and in the transition sections between gage and grip areas. Stress concentrations build within these areas and at the grips during testing, which can result in premature failures that underestimate true strength. Also, due to the high stiffness of ceramics, sample alignment must be precise to ensure that bending and other stress states do not cause premature failure of the specimens (*6*). Ceramic single lap joints may be used in a standard compressive shear test, but care must be taken to eliminate the tensile stress modes caused by bending during bond strength measurements (*7–9*). Tensile testing of bonded ceramic assemblies has been accomplished by loading circular butt joints in a purely axial direction, which requires precision sample machining and subsequent alignment in the testing fixture (*10*).

A second critical aspect to adhesive bonding that is often taken for granted is surface preparation and cleaning ceramic substrates. Amara et al. were able to determine the critical strain energy release rate (G_c) of the adhesive bond through finite-element analysis, but the effect of the ceramic surface treatment was limited to removal of contamination by exposure to an air atmosphere at 800 °C (*11*). While aggressive thermal cleaning treatments of ceramic surfaces are certainly effective, standard practices applied toward metals, such as sandblasting, are potentially easier to implement and more cost effective.

The third critical component to adhesive bonding is the durability of the bond line against environmental exposure. Simultaneous exposure of bonded ceramic joints used in structural engineering applications to thermal/moisture conditions during static loading using the aforementioned test methodologies has not been thoroughly explored.

An area of study where great focus has been placed on the moisture durability of adhesive bonding of ceramics is dental applications (*12–14*). The adhesive bonding of ceramic orthodontic inserts presents unique challenges that are not encountered in structural engineering applications. Surface preparation methods employed to improve the bonding between the resin and ceramic can involve a combination of techniques including acid etch cleaning, sandblasting with aluminum oxide particles, intraoral sandblasting using tribochemical silica coatings, and applying silane coupling agents, which may be applied in vitro (*15–17*). Furthermore, the preceding surface treatments must not result in bond strengths so great as to impart damage to the underlying tooth should there be a need for subsequent removal and repair (*15*, *18*). Determining fracture mechanics–based strain energy release rates across the interface of dental bonds has been accomplished using a four-point bending technique, but the debonded area at failure was relatively small (*19*, *20*). The limited bond surface area of these mechanical testing methods has the potential to introduce large amounts of experimental error, which must be compensated by analyzing statistically large sample sets. Environmental exposure is often limited to mechanical testing on the millimeter scale of bonded ceramic blocks or extracted human teeth that have been exposed to repeated thermal cycling in water between 5 and 55 °C (*21*, *22*). While there is no doubt as to the success of dental ceramic-bonding techniques and surface pretreatments, research efforts in this field of study are justifiably narrowly focused to clinical chairside techniques and are not concerned with broader engineering applications.

The goal of this research is to obtain critical strain energy release rates of bonded ceramic joints for structural engineering applications while undergoing concurrent environmental conditioning. To achieve this purpose, an asymmetric wedge test configuration has been designed where a compliant nonceramic adherend is bonded to a nondeformable ceramic base. This experimental methodology results in only the compliant nonceramic adherend experiencing bending deformations upon insertion of the wedge. As the testing geometry is fairly simple, elaborate machining is avoided due to a readily available selection of ceramics from commercial vendors that will fulfill acceptable dimensional requirements without additional modification. Additionally, the principal fracture mechanics of the asymmetric wedge test are well known with a methodology heritage originating with the splitting strength of mica experiments conducted in the 1930s through the recent use of asymmetric double cantilever beam testing to measure the fracture toughness of polymer interfaces (*23*, *24*). As is the case for symmetric wedge tests designed for bonded metals, an asymmetric wedge test is ideally suited for measuring the effect of ceramic surface treatments on bond strength and durability through simultaneous exposure to elevated humidity levels and temperatures. Furthermore, the large ceramic surface area presented in this testing geometry is conducive to abrasive sandblasting cleaning techniques

2

adopted for metals. While sandblasting ceramics is accepted by the dental community as an adhesion-promoting process, it is not known if abrasive surface damage will degrade the mechanical properties of the ceramic in high-stress, large-strain structural engineering applications.

2. Experimental

2.1 Asymmetric Wedge Test Analysis

Unlike symmetric double cantilever beam specimen configurations, which are associated with pure mode I tensile loading, asymmetric geometries provide an avenue for introducing mode II shear contributions to the system. The strain energy release rate, G, for the asymmetric wedge configuration is given by the following expression:

$$G = G_I + G_{II} = \frac{3Eh^3}{8a^4}\Delta^2,$$ (1)

where E is the modulus of the compliant adherend, h is the thickness of the compliant adherend, Δ is the displacement at the loading point, and a is the crack length from the loading point (25).

The strain energy release rates for asymmetrically loaded double cantilever beam geometries are well known and are often dependent on the mechanical properties of the adherends and the specimen geometry (26–28). As the system becomes increasingly asymmetric, a greater degree of mode II loading is introduced into the system (29). Mode mixity of loading also influences the locus of failure and the directional stability of advancing cracks (30, 31). As the percentage of mode II loading increases, the locus of failure shifts from cohesive in the adhesive to interfacially along the adherend surface. At small ratios of G_{II} to G_I ($G_{II}/G_I <3\%$), the crack front will oscillate between the adherend interfaces at regular intervals proportional to the thickness of the adhesive. At larger G_{II} to G_I ratios ($G_{II}/G_I <14\%$), the crack front has increased directional stability and propagates along one adherend interface only. The asymmetric wedge configuration studied for this research is the upper bound for double cantilever beam mixed-mode loading, where one adherend does not deflect upon insertion of the wedge. As this limit is approached, ~38% of the compliant bending energy is transmitted to the crack in plane shear, which is advantageous for investigating bond failure at the ceramic-adhesive interface.

2.2 Asymmetric Wedge Test Sample Fabrication and Testing

To eliminate ceramic machining, commercially available square alumina tiles with standard dimensions of $10.16 \times 10.16 \times 2.54$ cm were used as the substrate. The epoxy adhesive used for the study is estimated to have an initial G_c value ranging from 1000 to 2000 J/m^2. A wedge

thickness (Δ) of 3.18 mm, titanium thickness (h) of 3.18 mm, and titanium modulus (E) of 113.8 GPa requires an initial crack length (a) of ~52 to 43 mm calculated from equation 1. The calculated initial crack length was nearly half the length of the commercially alumina tiles available for this research and would limit the crack growth that could occur during subsequent environmental exposure. Therefore, it was decided to simply butt two tiles together end on end with the first tile serving as a loading base for the wedge and the second tile purely for adhesive bonding (see figure 1). The specific details of the sample fabrication are described in the following sections.
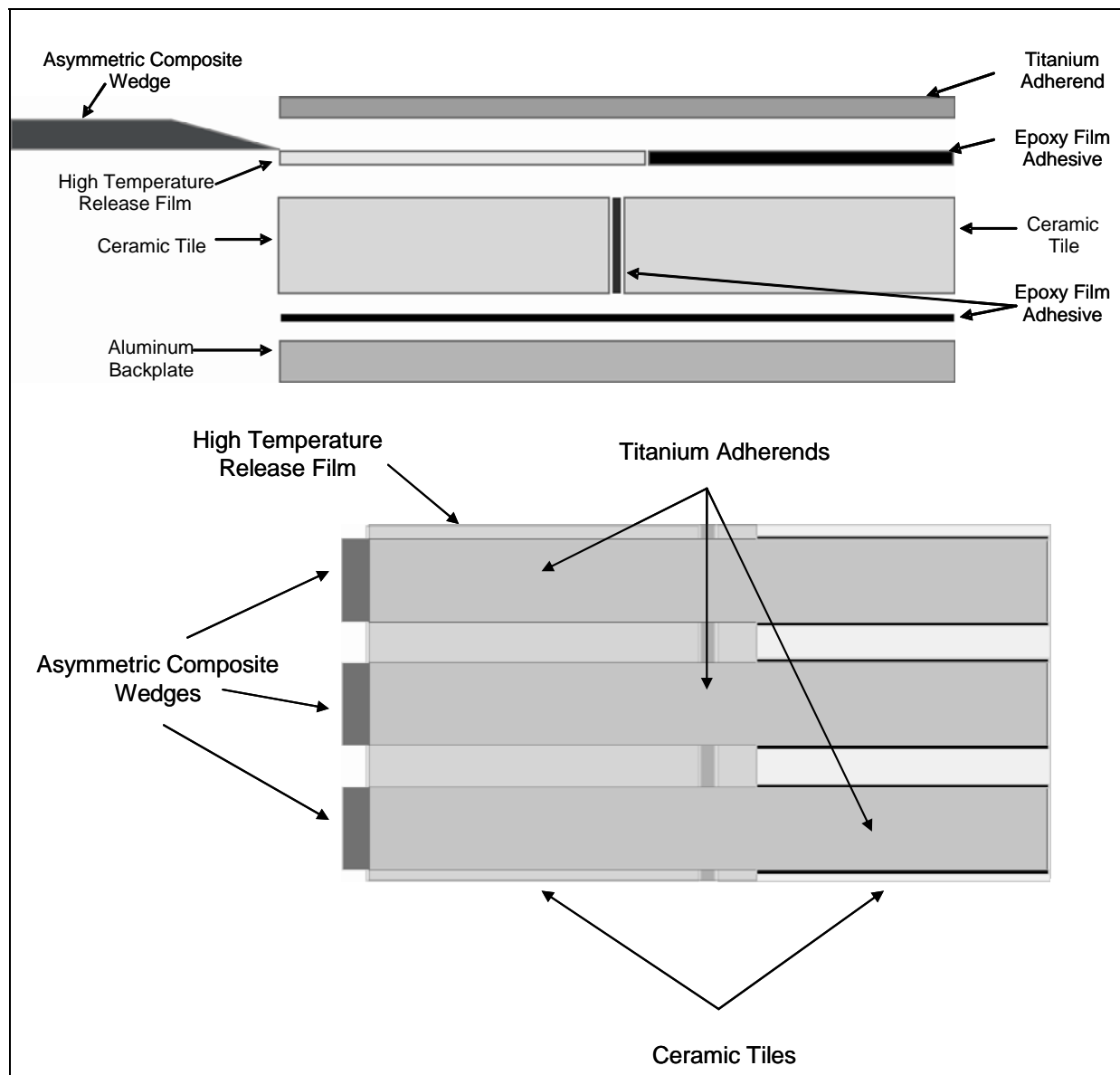

Figure 1. Experimental setup of titanium bonded to alumina using the asymmetric wedge configuration.

2.2.1 Bonding Alumina to the Backing Plate

The first step involves the adhesive bonding of two AD 995 alumina ceramic tiles (Coorstek, Golden, CO) to a 19.1- × 15.2- × 0.95-cm rectangular aluminum alloy backing plate. The alumina tiles must be bonded to the backing plate to maintain planar integrity while the titanium is loaded in bending by the wedge. Single faces of the ceramic tiles and the aluminum backing plate were degreased using acetone (AT) and sandblasted with 80-μm grain-size aluminum oxide particles (Electro Abrasives Corporation, Buffalo, NY). A sandblast machine (Econoline model RA 60 × 48 CB, Grand Haven, MI) was used at 0.69 MPa of compressor oil-free air pressure at a working distance and blast angle of ~5 cm and 90° normal to the surface, respectively, until the surfaces were visibly uniform in appearance. The residual surface sand was removed from the alumina surface by blowing with a stream of nitrogen gas. The cleaned surfaces were then treated with AC-130 sol-gel (A-C-Tech, Garden Grove, CA) using manufacturer-recommended 1-hr ambient drying conditions to promote covalent bonding with the epoxy film adhesive. The two ceramic tiles and aluminum backing plate were bonded using two layers of FM 94 K epoxy film adhesive (nominal weight = 146 g/m^2, nominal thickness = 0.15 mm, knit carrier, Cytec Engineered Materials, Havre de Grace, MD). Additionally, two layers of adhesive at the butt joint between the tiles were used to prevent the ceramic tiles from cracking upon cool down due to the CTE differences between the ceramic tiles (8.2 μm/m°C), backing plate (23 μm/m°C), and adhesive (>90 μm/m°C*). The bonded assembly was then cured at 121 °C for 2 hr in a vacuum bag under ~100 kPa vacuum pressure. The samples were then allowed to slowly cool to room temperature under vacuum pressure while the oven remained closed.

2.2.2 Bonding Titanium to the Alumina

The remaining exposed faces of alumina tiles were either rinsed with AT or sandblasted using the previously described methodologies prior to the application of the sol-gel adhesion promoter. Once treated with sol-gel, the loading tile was taped with a polyimide release film. The release film was taped in a parallel line to the tile-to-tile butt joint ~6.35 mm onto the second bonding tile to prevent the seam from influencing initial crack growth during test loading.

Titanium adherends were machined from Ti$_6$Al$_4$V alloy into 20.32- × 2.54- × 0.318-cm rectangular strips and sandblasted with 80-μm aluminum oxide particles at 0.69-MPa air pressure until the surfaces were visibly uniform in appearance. The loose surface sand particles were then removed by blowing with nitrogen gas followed by immediate treatment with the sol-gel, which was followed by a 1-hr ambient drying cycle. As the goal of this research is to examine the durability of the ceramic-adhesive bond, the additional precaution of treating the titanium with BR6747-1 primer (Cytec Engineered Materials, Anaheim, CA) was taken to ensure further protection of the titanium-adhesive interface during environmental exposure. The primer was

---

*Estimated CTE at cure temperatures exceeding the glass transition temperature of the adhesive.

applied using a painting technique, and the excess was removed by blowing with a gentle stream of nitrogen gas. The primer was dried at ambient conditions for 1 hr followed by 121 °C for 1 hr.

The titanium-adherend strips were bonded to the top face of the alumina tiles using two layers of epoxy film adhesive. The epoxy film adhesive was cut to match the length and width dimensions of the combined end-to-end joined tiles. Three titanium adherends, spaced ~6.35 mm apart, were placed parallel to each other on the alumina substrate. The sample assemblies were placed in a vacuum bag, and the adhesive was cured at 121 °C for 2 hr under an applied vacuum of ~100 kPa. As was the case for the initial bonding of the backing plate, the samples were allowed to slowly cool to room temperature under vacuum pressure while the oven remained closed. The excess epoxy adhesive at the free edges along the lengths of the titanium adherends was cleaned with a small hand-held electric grinding wheel to remove excess adhesive flow. The cleaned edges were solvent rinsed with AT and painted with a two-part epoxy-based white paint primer. This water-resistant white coating provided excellent optical contrast for monitoring crack growth during loading and environmental exposure.

2.2.3 Asymmetric Wedge Machining and Test Sample Loading

Asymmetric wedges measuring $5.08 \times 2.54 \times 0.635$ cm with a single 45° angle cut at one end were fabricated from glass-reinforced composite end-tab stock using an angle cutter mounted to a milling machine. The asymmetric wedges were then inserted between the alumina tile and titanium adherend, on top of the polyimide film precrack, using a hydraulic press to a fixed displacement. This provided an initial G_c loading value of ~2000 J/m^2. For hot/wet durability testing, the loaded test samples were immersed in distilled water baths held at a constant temperature of 60 °C. The amount of crack growth for each specimen was measured periodically over the course of ~3 weeks of immersion using a digital vernier caliper. A total of two complete asymmetric wedge fixtures were fabricated for each alumina surface treatment condition with each fixture containing three individual samples. Upon completion of the moisture exposure, any samples that had not failed spontaneously were manually debonded with a pry bar, and the degree of cohesive/adhesive failure was qualified visually.

2.3   X-ray Photoelectron Spectroscopy (XPS) Analysis

X-ray photoelectron spectroscopy (XPS) was used to examine the surface chemistry of the alumina ceramic following degreasing in AT and sandblasting. Sections of alumina were machined (Bomas Machine Specialties, Somerville, MA) into 10- $\times$ 10- $\times$ 2-mm squares to meet the dimension handling limits of the XPS analyzer chamber and sample mounting fixture. The small XPS alumina sample squares were cleaned, following identical procedures as the larger tiles, with the use of a small clamping vice to prevent loss from the air pressure of the sandblasting machine and nitrogen gas stream used to remove residual sand particles. A Kratos Ultra XPS system (Manchester, UK), equipped with a hemispherical analyzer, was used to

characterize the near-surface composition of the alumina substrates. A 196-W monochromatic Al Kα (1486.7 eV) beam irradiated a 1- × 1/2-mm spot. All spectra were taken at a 2×10^{-9} torr vacuum environment or better. Survey and elemental high-resolution scans were taken at pass energy = 80 eV for 2 min and pass energy = 20 eV for 2–8 min depending on S/N, respectively. The photoemission spectra measure quantitative (atomic surface concentrations) and qualitative (functional group identification) chemical information. A hybrid electrostatic and magnetic lens column with an integral coaxial charge neutralizer was employed to maintain uniform surface charge for the exact spot under examination. Kratos Vision 2 software was utilized for all data analysis.

2.4 Flexural Strength Evaluation

Flexural strength testing was conducted on the alumina ceramic in accordance with the ASTM C 1161 four-point bending method to determine the mechanical effects of sandblasting (*32*). Standard "B" size (3 × 4 × 50 mm) rectangular flex bar specimens were machined (Bomas Machine Specialties, Somerville, MA) from sections of the alumina tile. The flexural strengths were measured following the standard AT rinse and sandblasting surface treatments to determine the effects of abrasive damage. The testing was carried out using an Instron 1123 (Norwood, MA) electromechanical load frame. The alumina flexure bars were loaded into a fully articulating four-point bend fixture with the 4-mm treated surface facing the tensile (bottom) direction. The inner and outer support spans were 20 and 40 mm, respectively. A preload of 20 N was applied to ensure that the sample was level and that no point contacts between the rollers and the specimen were present. Running in load-control mode and using a 5-kN reversible load transducer, the specimens were loaded at a crosshead displacement rate of 0.5 mm/min, ensuring a flexural strain rate of 1×10^{-4} s^{-1}.

The flexural strength, *S*, was calculated using the following equation:

$$S = \frac{3PL}{4bd^2} \ , \tag{2}$$

where *P* is the load at failure, *L* is the length of the outer support span, *b* is the specimen width, and *d* is the specimen thickness.

The flexural strengths were also measured for sandblasted samples that had also undergone subsequent sol-gel treatment and adhesive bonding to examine any possible healing effects. Treatment of the sandblasted flex bars using the sol-gel followed identical procedures as described previously. The epoxy film adhesive was bonded as a single layer using a heated press at 121 °C for 2 hr at 100-kPa pressure to mimic the vacuum pressures used in the bagging process for the asymmetric wedge samples. Thirty valid four-point flexural strength tests for each surface preparation were conducted.

A Philips FEI XL series environmental scanning electron microscope (Netherlands) was used for fractography of the failed specimens to more accurately capture the intrinsic flaw population in

the as-received samples and the strength-dominating flaw population for each of the different surface treatments.

---

3.   Results and Discussion

3.1   Adhesive Bond Durability

Figures 2 and 3 show the plots of the crack length and fracture energy, respectively, as a function of moisture exposure time for the AT- and sandblast-cleaned (prior to application of the sol-gel adhesion promoter) asymmetric wedge assemblies. In figures 2 and 3, a number of the samples that were AT rinsed only prior to applying the sol-gel experienced complete spontaneous failure during the course of the study, as indicated by the circled data points. These spontaneous failures were not included in the calculations of average crack length or error. Sandblasting resulted in no spontaneous failures. All samples studied were initially loaded to average initial fracture energies of 2027 ± 176 J/m^2. The crack length plots show that the largest crack growth for both the AT and sandblasted samples occurred within the first 100 hr of moisture exposure. While the increases in crack length, and resulting decreases in fracture energy, were greatest for the AT samples, the remaining crack growth for both the AT and sandblasted samples remained similar to each other at times >100 hr. However, the moisture exposure of the AT-cleaned samples resulted in noticeably inconsistent adhesive bond durability, with either seemingly very good or very poor performance observed. Exactly 50% of the AT samples that were tested failed spontaneously during moisture exposure, as indicated by the circled data points in figures 2 and 3. Furthermore, the spontaneous failures of the AT-cleaned samples were apparent random events and not biased toward longer exposure times as might be expected.

During sample preparation, the sol-gel adhesion promoter was observed to wet the surface of the sandblast-cleaned alumina much more evenly than the AT-cleaned alumina. Therefore, the solvent rinsing used in the AT-cleaning procedure yielded regions of varying sol-gel coupling to the surface of the ceramic, which resulted in the inconsistent durability. For comparative purposes, if the ceramic is cleaned by solvent rinsing or sandblasting prior to adhesive bonding without the subsequent use of the sol-gel adhesion promoter, then complete 100% failure will occur in all samples within 12 hr at the temperature and moisture conditions chosen for this study. The larger experimental scatter in the crack length growth and fracture energy for the sandblast-cleaned samples was the result of fixture-to-fixture variation as the three individual asymmetric wedge samples within each individual fixture showed low experimental variation. One premise of the asymmetric wedge test is the potential to reduce the amount of experimental scatter typically observed during testing of very small dentistry-derived samples. The larger than expected experimental error recorded during these experiments is probably more attributable to inconsistencies with the application of the sol-gel rather than the asymmetric wedge test design.
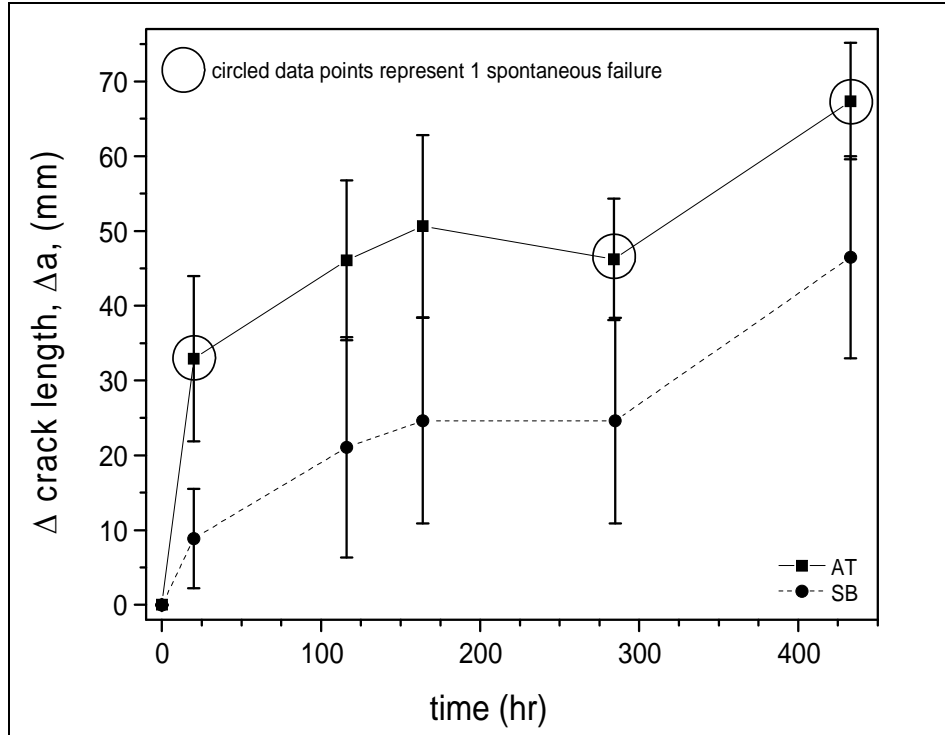
8

Figure 2. Average crack length growth for asymmetric wedge samples when immersed in water at a constant temperature of 60 °C as a function of time.
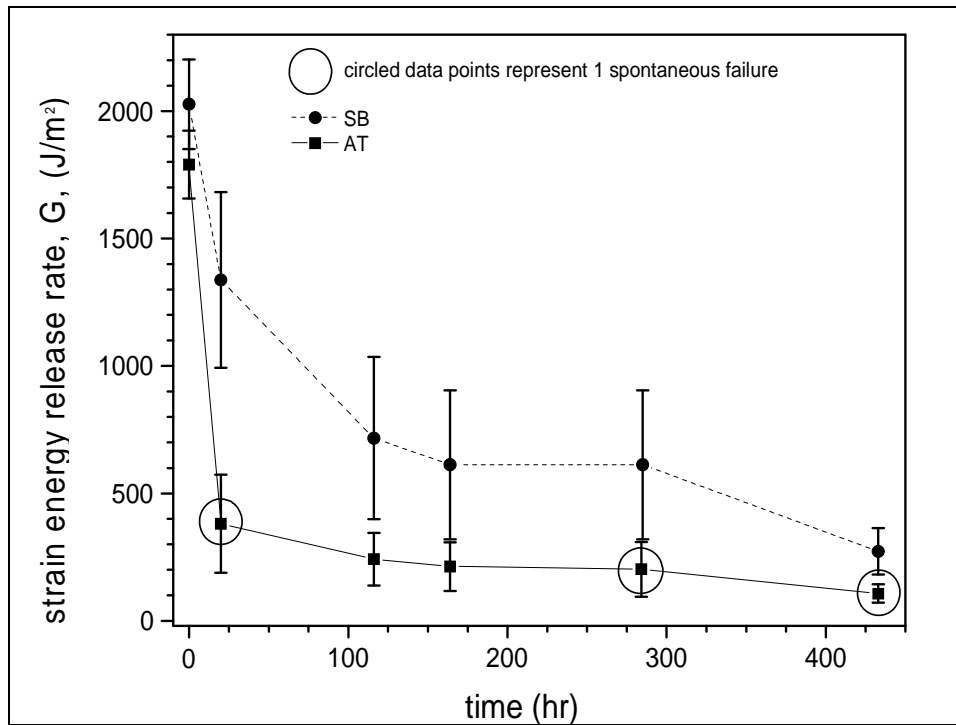

Figure 3. Average strain energy release rates for asymmetric wedge samples when immersed in water at a constant temperature of 60 °C as a function of time.

After 433 hr of testing, all specimens that had not failed spontaneously were manually failed to discern the type of failure exhibited at the ceramic/adhesive interface. Figure 4 shows the ceramic and titanium failure surfaces for the AT- and sandblast-treated samples with the regions of initial wedge insertion, exposure to moisture, and final manual failure indicated. The failure surface of the titanium adherends corresponds to the bottom sample failure surfaces on the alumina ceramic. Also note that the top AT sample failed prematurely during exposure. The initial wedge insertion and loading resulted in cohesive failure within the epoxy film adhesive for all of the AT- and sandblast-treated samples, as residual film adhesive is clearly evident on both the titanium and alumina adherends. The fracture mechanics of the asymmetric wedge configuration would seem to predict an initial failure at the film adhesive/alumina interface, but the strength of the film adhesive may have been reduced by curing under a vacuum pressure of 100 kPa rather than the manufacturer's recommended autoclave pressure of 275 kPa, as evident by the incomplete wetting of the adhesive's knit carrier cloth. Upon exposure to moisture at an elevated temperature, the locus of failure shifts to adhesive at the film adhesive/alumina interface. It is unknown if the exact locus of failure occurred within the alumina, at the alumina/sol-gel interface, or sol-gel/film adhesive interface as the sample dimensions greatly exceeded the size capability of the XPS. Also note that the AT-treated samples that failed spontaneously during the course of the moisture exposure showed adhesive failure at the film adhesive/alumina interface along the entire remaining length the alumina tile.

3.2 XPS Analysis of Surface-Treated Alumina

While XPS analysis of the failure surfaces was not possible, studies of the cleaning procedure and sol-gel application using the 10- × 10- × 2-mm machined alumina squares provided insight to the bond durability results. XPS survey results for the alumina specimens subjected to AT and sandblast cleaning regiments are shown in figure 5. The carbon-aluminum ratio is an indication of how much carbon is present on the surface relative to alumina. A higher ratio indicates an excess of carbon. For the AT specimens, the carbon-aluminum ratio was 0.52. For the sandblasted specimens, the ratio dropped to 0.26, indicating a significant decrease in the amount of carbon on the surface of the alumina. Figures 6 and 7 show XPS high-resolution spectra of the C_{1s} peaks for the AT and sandblasted specimens, respectively. Note the drop in the peak intensity when the sample has been grit-blasted prior to sol-gel application. Sandblasting is advantageous because the removal of carbon, a surface contaminant, provides higher bonding between the silane coupling agent (γ-glycidoxypropyltrimethoxy silane [GPS] or sol-gel) and the virgin alumina surface. This maximizes the effectiveness of the silane coupling agent and results in stronger bond strength when the adhesive is cured on the surface. Table 1 gives XPS elemental atomic concentrations for several elements for several surface preparations. The specific sandblast machine reported in this research is used for multiple cleaning processes, including removal of fluorinated release agents from the bonding surfaces of fiber-reinforced composites. Therefore, contaminated sandblast particles were removed prior to use, and the interior of the blast chamber was wiped down using AT.
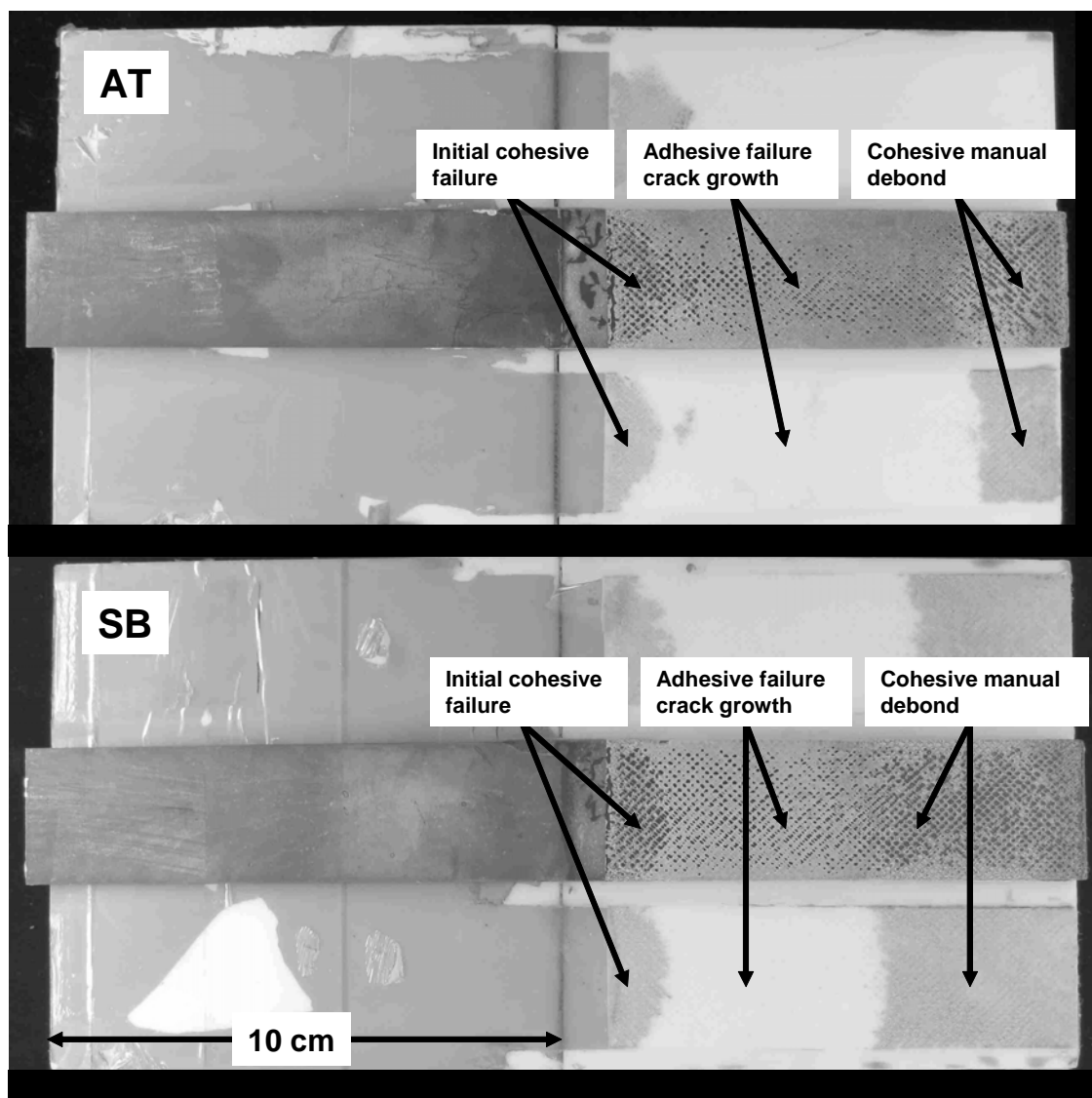
Figure 4. Failure surfaces of manually debonded asymmetric wedge samples after 433 hr of immersion in water at a constant temperature of 60 °C. (Note: SB = sandblasted.)

The interactions of traditional silane coupling agents, such as GPS, as epoxy adhesion promoters with aluminum substrates have been previously characterized by XPS analysis (*33*, *34*). These model studies of GPS/aluminum interactions indicate that this coupling agent should also be a model adhesion promoter for alumina ceramic adherends. Unpublished results obtained in the laboratory have verified that GPS is highly effective as an epoxy-compatible coupling agent for alumina ceramics. However, to promote condensation and cross-linking of the GPS to the substrate surface requires a post-bake thermal treatment at 93 °C for 60 min. As discussed in the experimental section, the thicker cross-section ceramic samples are prone to cracking upon cooldown when bonded to a metal backing plate due to the mismatch in CTE. Therefore, the
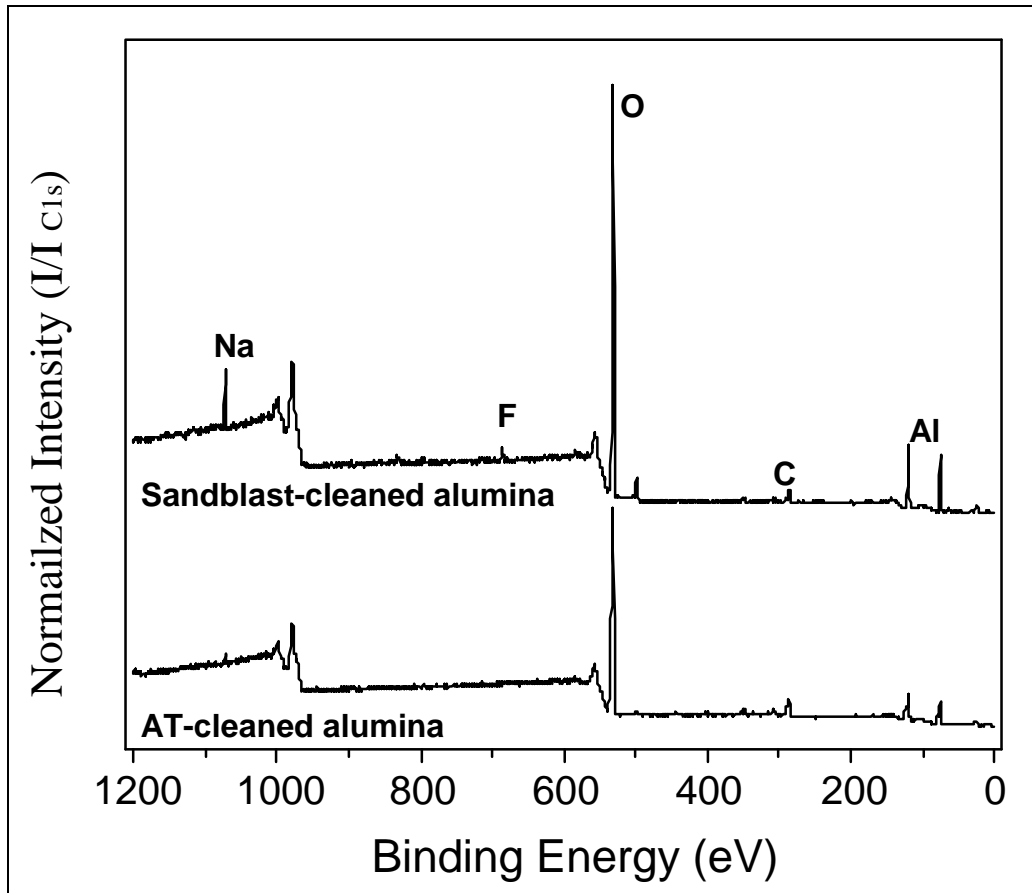
Figure 5. XPS survey results comparing the AT and sandblasting cleaning procedures of the
alumina ceramic. Curves shifted up for clarity.

sol-gel-based adhesion promoter was chosen to minimize the number of heat/cool cycles and reduce the risk of fracturing the ceramic. The sol-gel adhesion promoter formulation incorporates a zirconium isopropoxide additive that catalyzes condensation and cross-linking of GPS at room temperature (*35*, *36*).

3.3   Flexural Strength Testing Results

The characteristic strength of ceramic materials is largely governed by strength-limiting preexisting flaws, which can be introduced in the material during preprocessing, densification, or subsequent surface machining. Due to the high strength and low fracture toughness of ceramic materials, flaw volume tolerances are often extremely small, often on the order of a few cubic microns. Flaws located at the specimens' surface or internal volume are often the initiation sites for catastrophic failure. The size and location of these flaws vary from specimen to specimen, resulting in a large scatter of strength values and often failure types. Examples of internal flaw populations include pores caused by incomplete densification, agglomerates of secondary phases, and excessively large primary phase grains (*37*).
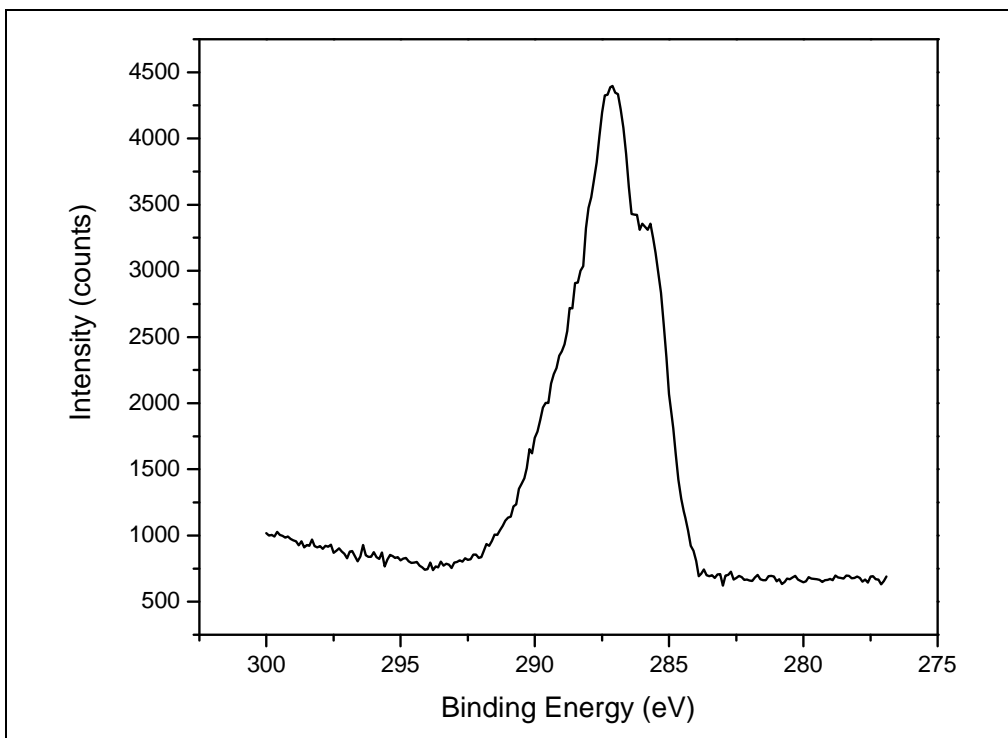
Figure 6. XPS high-resolution spectra of the C_{1s} peaks of the sol-gel-treated alumina ceramic after AT cleaning.
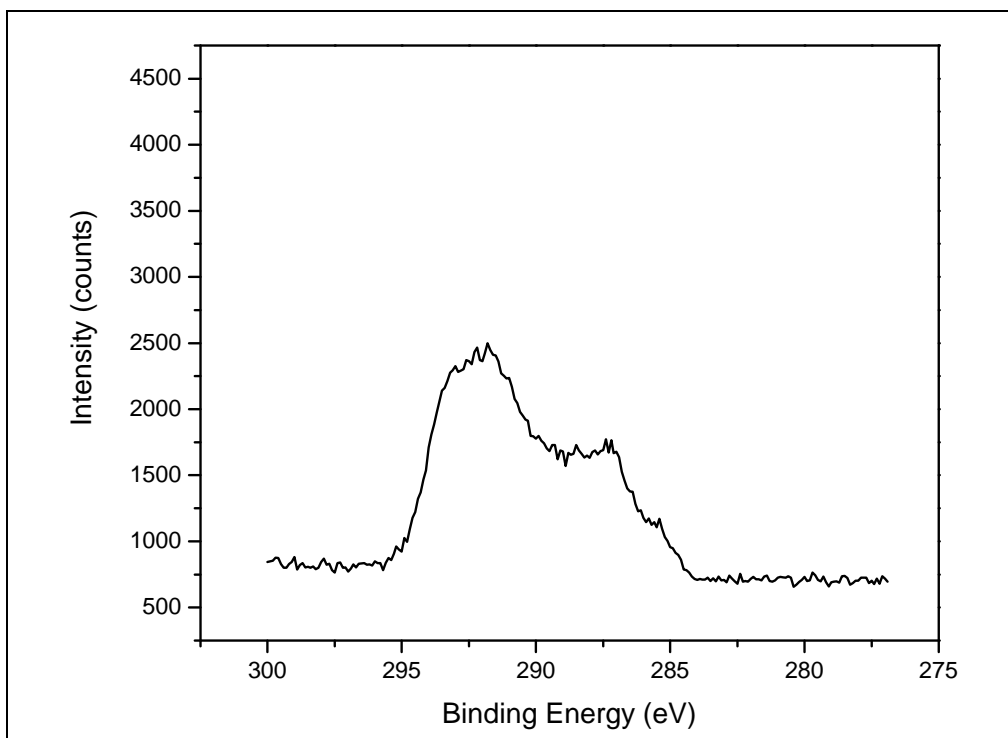

Figure 7. XPS high-resolution spectra of the C_{1s} peaks of the sol-gel-treated alumina ceramic after sandblast cleaning.

Table 1. XPS elemental atomic concentrations for surface analysis of the alumina following AT or sandblast cleaning with subsequent treatments of sol-gel adhesion promoter.

Element	AT Cleaning	AT Cleaning With Sol-Gel Application	Sandblast Cleaning	Sandblast Cleaning With Sol-Gel Application
Na 1s	0.48	0	2.50	0
F 1s	0	0	1.35	0
O 1s	48.04	33.71	51.08	44.49
C 1s	17.67	50.40	9.29	35.66
Zr 3d	0	2.67	0	0.45
Si 2p	0	7.07	0	0.97
Al 2p	33.76	6.15	35.72	18.46

Surface-cleaning regiments, such as sandblasting, can also affect the strength of the material by significantly altering an existing flaw population or by creating a new and dominant flaw population, which could possibly lead to significant degradations in strength. The four-point bend flexural test is ideally suited to track changes in the characteristic strength of the alumina ceramic due to sandblasting of the bonding surfaces. Any apparent increases in surface damage should lead to an observable increase in tensile failure modes. Weibull statistics are the commonly accepted means of quantifying the brittle mechanical behavior of ceramics and comparing strength values. The two-parameter Weibull distribution function denotes the failure probability that a material will fail when subjected to an applied stress, σ.

$$\ln \ln \left(\frac{1}{1-F} \right) = m \ln \sigma_f - m \ln \sigma^* , \tag{3}$$

where F is the failure probability, and σ^* is the characteristic strength.

The failure probability, F, is calculated for each specimen in the population using the estimation

$$F = \frac{n - 0.5}{N} , \tag{4}$$

where the strength data of N specimens are ranked from weakest to strongest with $n = 1$ denoting the weakest specimen. By plotting the natural log functions of F and σ_f, the Weibull modulus, m, and the characteristic strength, σ^*, can be found as the slope and y-intercept, respectively. These two Weibull parameters give insight into the strength and variability of flaw population within the experimental series. A high Weibull modulus indicates low variability in strength values, and a high intercept indicates a high characteristic strength.

Figure 8 shows the Weibull plot strength data for the alumina after undergoing the AT and sandblast surface-cleaning measures. The AT-cleaned ceramics had a characteristic strength of 291 MPa and a corresponding Weibull modulus of 42.0. This strength value is typical of similar alumina materials, and the relatively high Weibull modulus indicates a low variability in strength distribution. From the Weibull distribution, it is evident that there is only one dominant flaw population in the as-received ceramic. Fractography revealed that the locus of failure originated at the weaker tensile surfaces, as shown in figure 9. The semi-elliptical cracks intersecting the tensile surface of the specimen were caused by the abrasive nature of specimen machining of the bend bars. The AT surface-cleaning procedure used for adhesive bonding is a simple solvent rinse and should not contribute to the surface flaw population. The range of flaw sizes determined from fracture mechanics equations and fractography confirmation was 105–133.8 µm.
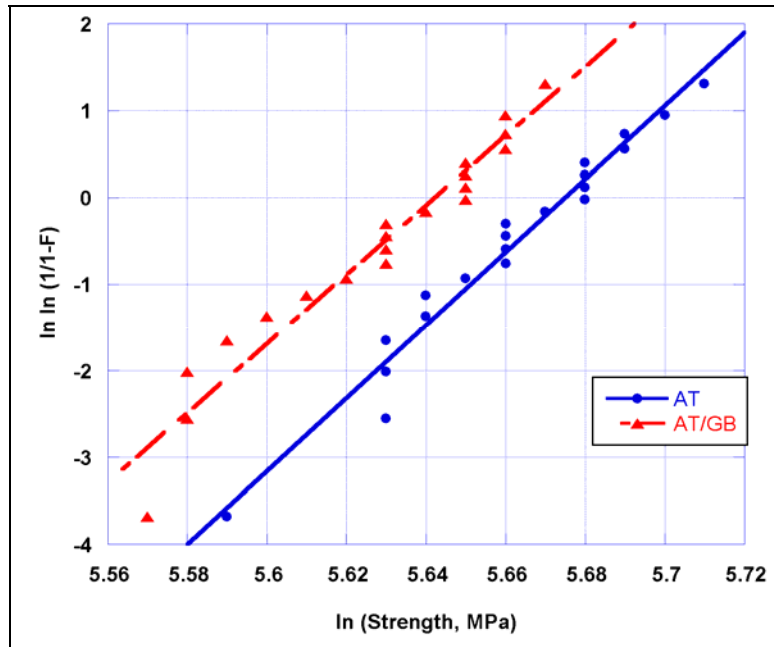

Figure 8. Weibull distribution for flexural strength of alumina that were surface cleaned by solvent rinsing in AT (•) or sandblasting (▲). Note that these samples were not treated with the sol-gel adhesion promoter after surface cleaning.

In the case of the sandblasted sample set, the characteristic strength drops to 282 MPa, and the Weibull modulus drops to 39.8 when compared to the AT-treated values, also shown in figure 8. This ~3% decrease in strength was most likely due to intensification of the preexisting surface flaws observed in the AT specimens. The impacting and abrasive nature of sandblasting imparts a tensile stress field with a maximum stress located below the surface of the material. The tensile stresses are relieved through the introduction of new surface defects or through growth of existing defects, both of which decrease the strength of the ceramic. Fractography of the sandblasted

specimens confirmed that the size of existing surface defects was increased by the sandblasting medium, as seen in figure 10. The range of flaw sizes determined from fracture mechanics equations and fractography confirmation was 116.2–140.1 µm.
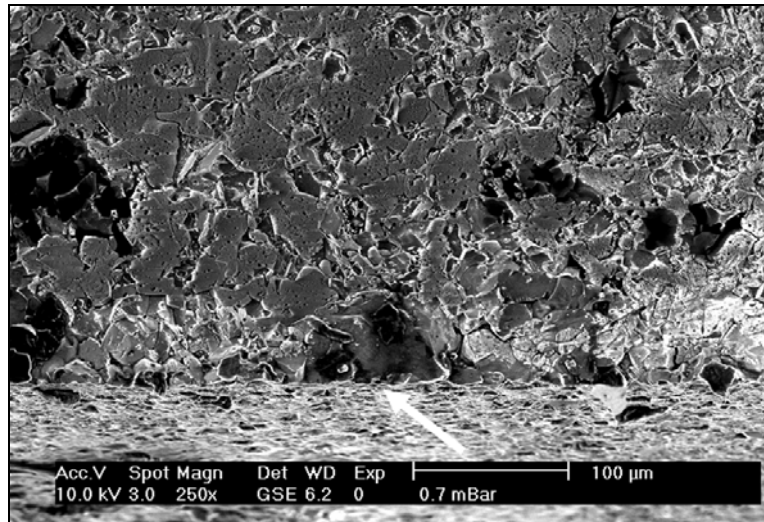

Figure 9. Fracture surface micrograph depicting a strength-limiting flaw in an AT alumina flexure specimen. The flaw, indicated by the white arrow, is a subsurface semi-elliptical crack induced by surface machining damage.
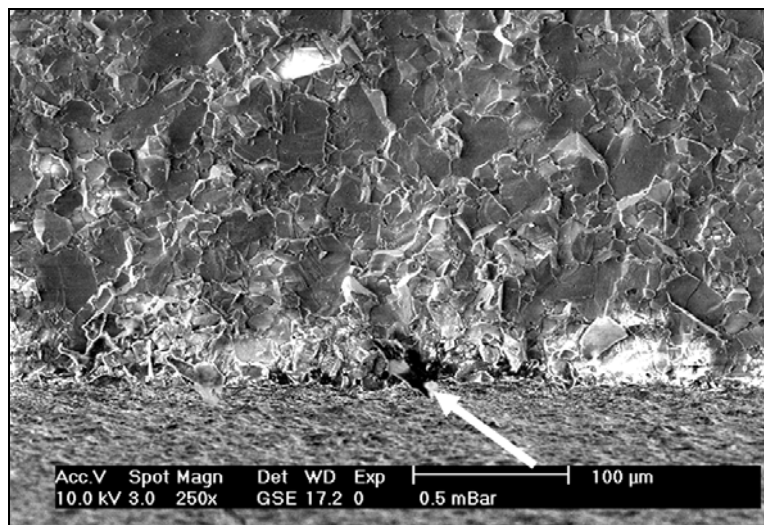

Figure 10. Fracture surface micrograph depicting a strength-limiting flaw in a sandblasted alumina flexure specimen. The white arrow indicates the origin of failure.

It is known that thin polymeric coatings applied to the surfaces of ceramics can yield increased strength. To investigate the contribution of the sol-gel adhesion promoter to ceramic strength, samples were subjected to sandblasting and sol-gel surface treatment (SB/SG). As seen from the Weibull plots in figure 11, the flexural strength of the SB/SG samples shows a marked "recovery" in strength when compared to the AT and sandblasted sample sets. The characteristic strength and Weibull modulus of these samples were 298.5 MPa and 32.2, respectively. The characteristic strength of the SB/SG alumina is slightly higher than the as-machined specimens, indicating that the sol-gel acts to suppress or negate the effects of the sandblasting and the original flaw population as well. The exact mechanism for this strengthening is not known. However, it is hypothesized that the sol-gel acts to either reduce stress concentrations associated with surface asperities or enter surface cracks to blunt the crack tips from the maximum stresses during loading.
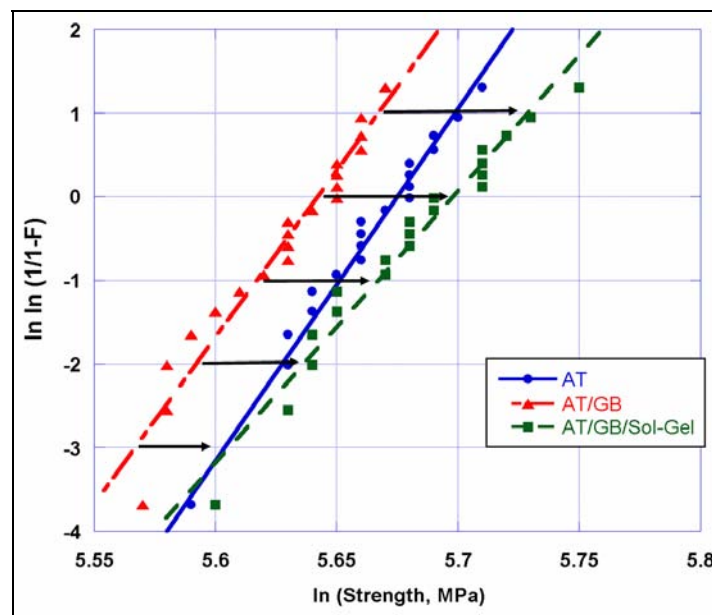
Figure 11. Weibull distribution for flexural strength of AT,
sandblasted, and SB/SG flexural strength specimens.
Note the recovery in flexural strength of the SB/SG
specimens after the sol-gel treatment was applied to
the tensile surface.

While the sol-gel seemed effective in recovering strength, possible ceramic strength increases were investigated by applying FM 94 film adhesive to the tensile side of alumina flexure bars with either AT/SG or SB/SG surface cleaning. As shown in the Weibull plots of figure 12, the characteristic strength and Weibull modulus for both the AT/SG/FM 94 and SB/SG/FM 94 increased to 350 MPa and 37, respectively. The identical value of characteristic strength for the different surface preparations upon application of the film adhesive indicates that the previously observed dominant surface flaw population may become suppressed to the extent that a

secondary flaw population becomes active. Silane coupling agents and thin film adhesives act to negate the effects of surface machining and sandblasting, as long as the populated flaw sizes are within the range of those created during this work. Fractography of the FM 94-coated flexure specimens revealed that failure still originated at surface machining defects, although failure from orthogonal machining cracks was observed in addition to cracks parallel to the machining direction, as seen in figure 13.
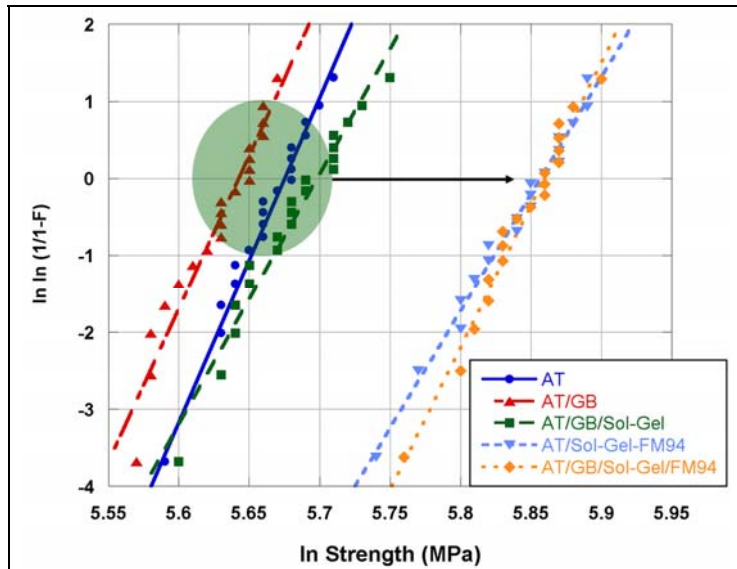
Figure 12. Weibull distribution for flexural strength of all alumina specimens. Note the increase in flexural strength when the film adhesive was applied to the tensile surface regardless of prior surface preparation, AT/SG/FM 94 and SB/SG/FM 94.
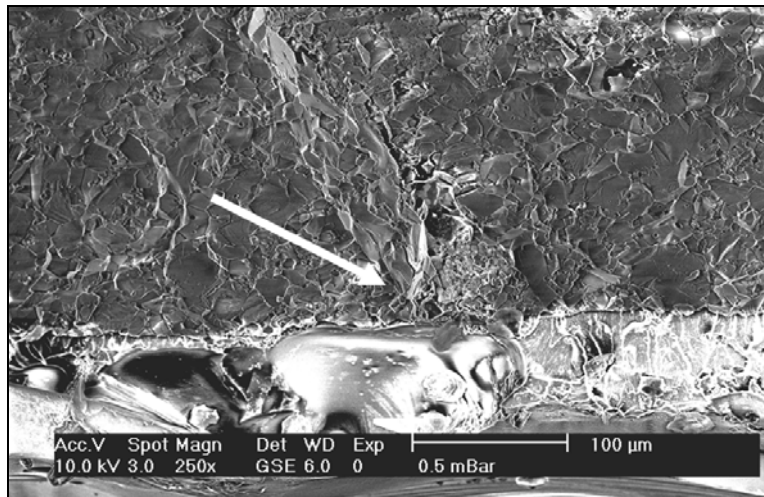
Figure 13. Fracture surface micrograph showing a strength-limiting orthogonal surface machining crack in an alumina flexure specimen coated with a single layer of film adhesive. The white arrow indicates the failure origin on the tensile surface.

18

4.   Conclusions

This research showed that the asymmetric wedge configuration is a valid testing methodology for evaluating the strength and durability of adhesively bonded ceramics. Furthermore, this testing configuration proved advantageous due to the absence of machine work needed for the ceramic, as the commercial as-received alumina geometry was acceptable. The crack tip loading of the asymmetric wedge configuration is well described by established fracture mechanics, which should prove more applicable to a variety of structural applications in comparison to more qualitative ceramic bonding schemes developed for the dentistry community. In addition, the contribution of mode mixity to the fracture mechanics drove the crack growth toward the ceramic substrate, which was the desired surface of interest.

The effects of different surface preparation techniques on bond durability were successfully evaluated using the asymmetric wedge configuration. The initial fracture energies for the sandblast-cleaned alumina samples proved slightly greater than simple AT rinsing as a surface-cleaning treatment. While differences in crack growth length between AT-rinsed and sandblasted specimens were consistent throughout the duration of the moisture exposure, the AT-rinsed samples did result in a number of spontaneous complete failures not experienced by the sandblasted samples. XPS analysis of the ceramic surfaces confirmed that sandblasting was more successful in removing ubiquitous carbon contamination from the alumina surface than solvent rinsing with AT. The XPS also showed that the sandblasted alumina surfaces promoted more effective coupling with the sol-gel adhesion promoter, which was presumably responsible for the increased durability consistency during moisture exposure.

Sandblasting the surface of the alumina ceramic resulted in a somewhat lowered flexural strength due to damage effects. However, applying sol-gel adhesion promoter was found to counter the negative effects of sandblasting and fully restore the strength of the ceramic. Subsequent application of the film adhesive actually increased the flexural strength of the ceramic. These results indicate that the film adhesive acts to reduce the contribution of the dominant surface flaw population to overall ceramic failure.

5. References

1. Anderson, C. E.; Morris, B. L. The Ballistic Performance of Confined Al2O3 Ceramic Tiles. *Int. J. Impact Engineering* **1992**, *12* (2), 167.

2. Franzen, R. R.; Orphal, D. L.; Anderson, C. E. The Influence of Experimental Design on Depth-of-Penetration (DOP) Test Results and Derived Ballistic Efficiencies. *Int. J. Impact Engineering* **1997**, *19* (8), 727.

3. Huang, X. G.; Gillespie, J. W.; Kumar, V.; Gavin, L. Mechanics of Integral Armor: Discontinuous Ceramic-Cored Sandwich Structure Under Tension and Shear. *Composite Structures* **1996**, *36* (1–2), 81.

4. Parvatareddy, H.; Dillard, J. G.; McGrath, J. E.; Dillard, D. A. Environmental Aging of the Ti-6Al-4V/FM-5 Polyimide Adhesive Bonded System: Implications of Physical and Chemical Aging on Durability. *J. Adhes. Sci. Technol.* **1998**, *12* (6), 615.

5. Chin, J. W.; Wightman, J. P. Surface Characterization and Adhesive Bonding of Toughened Bismaleimide Composites. *Comp. Part A: Appl. Sci. and Manufacturing* **1996**, *27* (6), 419.

6. Lawn, B. *Fracture of Brittle Solids;* 2nd ed.; Cambridge University Press: New York, 1993.

7. Baziard, Y.; El Abdi, R.; Amara, D.; Petit, J. A.; Levallois, F. Study of Critical Failure Parameters for an Adhesive-Bonded Single Lap Joint With Ceramic Adherends. *Int. J. Adhesion and Adhesives* **1995**, *15* (3), 155.

8. Levallois, F.; El Abdi, R.; Baziard, Y.; Petit, J. A. Study of the Crack Deviation Angle in Adhesive Ruptures of Ceramic Adhesively-Bonded Assemblies. *J. Adhes.* **1997**, *60* (1–4), 1.

9. Amara, D.; Levallois, F.; Baziard, Y.; Petit, J. A. Study of a Single-Lap Compression-Shear Test for Brittle Substrates Bonded With a Structural Adhesive. *J. Adhes. Sci. Technol.* **1996**, *10* (11), 1153.

10. Amara, D.; Hassoune, B.; El Abdi, R.; Baziard, Y.; Petit, J. A. A New Tensile Rupture Test for the Mechanical Characterization of an Adhesively-Bonded Structural Ceramic Assembly. *J. Adhes. Sci. Technol.* **1998**, *12* (10), 1029.

11. Levallois, F.; Helt, S.; Baziard, Y.; Petit, J. A. Structural Adhesive Bonding of Sintered Silicon Carbide (SSiC) Subjected to Thermal Treatment in Air Atmosphere. *J. Adhes. Sci. Technol.* **1999**, *13* (2), 273.

12. Blatz, M. B.; Sadan, A.; Kern, M. J. Resin-Ceramic Bonding: A Review of the Literature. *Prosthetic Dentistry* **2003**, *89* (3), 268.

13. Wolfart, M.; Lehmann, F.; Wolfart, S.; Kern, M. Durability of the Resin Bond Strength to Zirconia Ceramic After Using Different Surface Conditioning Methods. *Dental Materials* **2007**, *23* (1), 45.

14. Kitoh, S.; Suzuki, K.; Kiyohara, T.; Kurita, K. Adhesive Monomers to Dental Ceramics. I. Evaluation of <I>N</I>-Substituted 3-Amino-2-Hydroxypropyl Methacrylates as Adhesives for Calcium Metaphosphate Crystalline Glass-Ceramic. *J. Appl. Polym. Sci.* **1992**, *45* (8), 1329.

15. Atsu, S. S.; Gelgor, I. E.; Sahin, V. Effects of Silica Coating and Silane Surface Conditioning on the Bond Strength of Metal and Ceramic Brackets to Enamel. *Angle Orthodontist* **2006**, *76* (5), 857.

16. Della Bona, A.; Anusavice, K.; Hood, J. A. A. Effect of Ceramic Surface Treatment on Tensile Bond Strength to a Resin Cement. *Int. J. Prosthodontics* **2002**, *15* (3), 248.

17. Kern, M.; Wegner, S. M. Bonding to Zirconia Ceramic: Adhesion Methods and Their Durability. *Dental Materials* **1998**, *14* (1), 64.

18. Newman, S. M.; Dressler, K. B.; Grenadier, M. R. Direct Bonding of Orthodontic Brackets to Esthetic Restorative Materials Using a Silane. *Am. J. Orthodontics and Dentofacial Orthopedics* **1984**, *86* (6), 503.

19. Homann, F.; Waddell, J. N.; Swain, M. V. Influence of Water, Loading Rate and Bonder on the Adhesion of Porcelain to Titanium. *J. Dentistry* **2006**, *34* (7), 485.

20. Charalambides, P. G.; Lund, J.; Evans, A. G.; McMeeking, R. M. A Test Specimen for Determining the Fracture Resistarim of Bimaterial Interfaces. *J. Appl. Mechanics - Transactions of the ASME* **1989**, *56* (1), 77.

21. Andreatta Filho, O. D.; Bottino, M. A.; Nishioka, R. S.; Valandro, L. F.; Leite, F. P. P. Effect of Thermocycling on the Bond Strength of a Glass-Infiltrated Ceramic and a Resin Luting Cement. *J. Appl. Oral Sci.* **2003**, *11* (1), 61.

22. Hosoya, Y.; Kawada, E.; Liu, J.; Oda, Y.; Marshall, G. W. Micro-Tensile Strength of Sound Primary Second Molar Dentin. *J. Mater. Sci.* **2005**, *40* (23), 6181.

23. Obreimoff, J. W. Splitting Strength of Mica. *Proc. R. Soc. London, Ser. A* **1930**, *127* (805), 290.

24. Bernard, B.; Brown, H. R.; Hawker, C. J.; Kellock, A. J.; Russel, T. P. Adhesion of Polymer Interfaces Reinforced With Random and Diblock Copolymers as a Function of Geometry. *Macromolecules* **1999**, *32* (19), 6254.

25. Tada, H.; Paris, P. C.; Irwin, G. R. *The Stress Analysis of Cracks Handbook*, 3rd ed.; ASME Press: New York, 2000; pp 677.

26. England, A. H. A Crack Between Dissimilar Media. *J. Appl. Mechanics* **1965**, *32* (2), 400.

27. Erdogan, F. Stress Distribution in Bonded Dissimilar Materials With Cracks. *J. Appl. Mechanics* **1965**, *32* (2), 403.

28. Rice, J. R. Elastic-Plastic Fracture Mechanics Concepts for Interfacial Cracks. *J. Appl. Mechanics* **1988**, *55* (1), 98.

29. Xiao, F.; Hui, C. Y.; Kramer, E. J. Analysis of a Mixed-Mode Fracture Specimen. *J. Mater. Sci.* **1993**, *28* (20), 5620.

30. Chen, B.; Dillard, D. A. The Effect of the T-stress on Crack Path Selection in Adhesively Bonded Joints. *Int. J. Adhesion and Adhesives* **2001**, *21* (5), 357.

31. Chen, B.; Dillard, D. A.; Dillard, J. G.; Clark, R. L., Jr. Crack Path Selection in Adhesively Bonded Joints: The Roles of External Loads and Specimen Geometry. *Int. J. Fracture* **2002**, *114* (2), 167.

32. ASTM C 1161. Standard Test Method for Flexural Strength of Advanced Ceramics at Ambient Temperature. *Annu. Book ASTM Stand.* **2008**.

33. Rattana, A.; Hermes, J. D.; Abel, M. L.; Watts, J. F. The Interaction of a Commercial Dry Film Adhesive With Aluminium and Organosilane Treated Aluminium Surfaces: A Study by XPS and ToF-SIMS. *Int. J. Adhesion and Adhesives* **2002**, *22*, 205.

34. Abel, M. L.; Joannic, R.; Fayos, M.; Lafontaine, E.; Shaw, S. J.; Watts, J. F. Effect of Solvent Nature on the Interaction of [Gamma]-Glycidoxy Propyl Trimethoxy Silane on Oxidised Aluminium Surface: A Study by Solution Chemistry and Surface Analysis. *Int. J. Adhesion and Adhesives* **2006**, *26*, 16.

35. Blohowiak, K. Y.; Osborne, J. H.; Krienke, K. A. Sol for Bonding Epoxies to Aluminum or Titanium Alloys. U.S. Patent 6,037,060, 14 March 2000.

36. Osborne, J. H.; Blohowiak, K. Y.; Taylor, S. R.; Hunter, C.; Biewagon, G.; Carlson, B.; Bernard, D.; Donley, M. S. Testing and Evaluation of Nonchromated Coating Systems for Aerospace Applications. *Progress in Organic Coatings* **2001**, *41* (4), 217.

37. Green, D. J. *An Introduction to the Mechanical Properties of Ceramics*; Cambridge University Press: New York, 1998; pp 328.

NO. OF
COPIES   ORGANIZATION

  1   DEFENSE TECHNICAL
(PDF   INFORMATION CTR
only)   DTIC OCA
         8725 JOHN J KINGMAN RD
         STE 0944
         FORT BELVOIR VA 22060-6218

  1   DIRECTOR
         US ARMY RESEARCH LAB
         IMNE ALC IMS
         2800 POWDER MILL RD
         ADELPHI MD 20783-1197

  1   DIRECTOR
         US ARMY RESEARCH LAB
         AMSRD ARL CI OK TL
         2800 POWDER MILL RD
         ADELPHI MD 20783-1197

  1   DIRECTOR
         US ARMY RESEARCH LAB
         AMSRD ARL CI OK PE
         2800 POWDER MILL RD
         ADELPHI MD 20783-1197

         ABERDEEN PROVING GROUND

  1   DIR USARL
         AMSRD ARL CI OK TP (BLDG 4600)

ABERDEEN PROVING GROUND

21   DIR USARL
      AMSRD ARL WM
        J MCCAULEY
      AMSRD ARL WM M
        J BEATTY
      AMSRD ARL WM MA
        M VANLANDINGHAM
        E ROBINETTE
        D PAPPAS
      AMSRD ARL WM MB
        T BOGETTI
      AMSRD ARL WM MC
        M MAHER
        M BRATCHER
      AMSRD ARL WM MD
        C YEN
        S GHIORSE
        E CHIN
        K DOHERTY
        J MONTGOMERY
        B SCOTT
        G GILDE
        P PATEL
        J LASALVIA
        J SANDS
        S WALSH
        J CAMPBELL
      AMSRD ARL WM TA
        C HOPPEL